

Balancing strength and plasticity of dual-phase amorphous/crystalline nanostructured Mg alloys

Jia-Yi Wang(王佳怡), Hai-Yang Song(宋海洋), Min-Rong An(安敏荣), Qiong Deng(邓琼), Yu-Long Li(李玉龙)

Citation: Chin. Phys. B . 2020, 29(6): 066201 . **doi:** 10.1088/1674-1056/ab84d5
Journal homepage: http://cpb.iphy.ac.cn; http://iopscience.iop.org/cpb

What follows is a list of articles you may be interested in

Anisotropic plasticity of nanocrystalline Ti: A molecular dynamics simulation

Minrong An(安敏荣), Mengjia Su(宿梦嘉), Qiong Deng(邓琼), Haiyang Song(宋海洋), Chen Wang(王晨), Yu Shang(尚玉)
Chin. Phys. B . 2020, 29(4): 046201 . **doi:** 10.1088/1674-1056/ab7188

Investigation of mechanical properties of twin gold crystal nanowires under uniaxial load by molecular dynamics method

Guo-Wei Zhang(张国伟), Zai-Lin Yang(杨在林), Gang Luo(罗刚)
Chin. Phys. B . 2016, 25(8): 086203 . **doi:** 10.1088/1674-1056/25/8/086203

ReaxFF molecular dynamics study on oxidationbehavior of 3C-SiC: Polar face effects

Sun Yu, Liu Yi-Jun, Xu Fei
Chin. Phys. B . 2015, 24(9): 096203 . **doi:** 10.1088/1674-1056/24/9/096203

Effects of tilt interface boundary on mechanical properties of Cu/Ni nanoscale metallic multilayer composites

Yang Meng, Xu Jian-Gang, Song Hai-Yang, Zhang Yun-Guang
Chin. Phys. B . 2015, 24(9): 096202 . **doi:** 10.1088/1674-1056/24/9/096202

Dynamic strength behavior of a Zr-based bulk metallic glassunder shock loading

Yu Yu-Ying, Xi Feng, Dai Cheng-Da, Cai Ling-Cang, Tan Ye, Li Xue-Mei, Wu Qiang, Tan Hua
Chin. Phys. B . 2015, 24(6): 066201 . **doi:** 10.1088/1674-1056/24/6/066201

Balancing strength and plasticity of dual-phase amorphous/crystalline nanostructured Mg alloys*

Jia-Yi Wang(王佳怡)[1,2], Hai-Yang Song(宋海洋)[1,†], Min-Rong An(安敏荣)[1], Qiong Deng(邓琼)[2], and Yu-Long Li(李玉龙)[2,‡]

[1] College of Material Science and Engineering, Xi'an Shiyou University, Xi'an 710065, China
[2] School of Aeronautics, Northwestern Polytechnical University, Xi'an 710072, China

(Received 2 February 2020; revised manuscript received 29 March 2020; accepted manuscript online 31 March 2020)

The dual-phase amorphous/crystalline nanostructured model proves to be an effective method to improve the plasticity of Mg alloys. The purpose of this paper is to explore an approach to improving the ductility and strength of Mg alloys at the same time. Here, the effect of amorphous phase strength, crystalline phase strength, and amorphous boundary (AB) spacing on the mechanical properties of dual-phase Mg alloys (DPMAs) under tensile loading are investigated by the molecular dynamics simulation method. The results confirm that the strength of DPMA can be significantly improved while its excellent plasticity is maintained by adjusting the strength of the amorphous phase or crystalline phase and optimizing the AB spacing. For the DPMA, when the amorphous phase (or crystalline phase) is strengthened to enhance its strength, the AB spacing should be increased (or reduced) to obtain superior plasticity at the same time. The results also indicate that the DPMA containing high strength amorphous phase exhibits three different deformation modes during plastic deformation with the increase of AB spacing. The research results will present a theoretical basis and early guidance for designing and developing the high-performance dual-phase hexagonal close-packed nanostructured metals.

Keywords: dual-phase Mg alloy, metallic glass, mechanical property, molecular dynamics simulation

PACS: 62.25.–g, 64.70.pe, 61.82.Bg, 31.15.xv **DOI:** 10.1088/1674-1056/ab84d5

1. Introduction

To a large extent, today's technological development depends on materials such as metals, semiconductors or ceramics. Nanocrystalline materials have considerable mechanical strength, ductility, and other properties compared with traditional coarse-grained materials.[1] However, to date, the regulatory mechanisms of the properties of nanocrystalline materials on a nanoscale, especially hexagonal close-packed (HCP) crystal materials, are still not clear. The in-depth understanding of these mechanisms is still a hot topic of basic research. Recently, a considerable number of researches reported that the properties of crystalline materials, such as mechanical strength, electric conductivity, optical properties, *etc*., can be controlled by some approaches.[2–6] On the one hand, their properties can be adjusted by modifying their chemical microstructures, such as introducing different phases or varying chemical compositions.[2,6] On the other hand, they can also be controlled by introducing lattice defects such as intercrystalline interfaces and dislocations.[3,4] At present, there are abundant achievements in the study of the mechanical properties and deformation mechanisms of nano-polycrystalline metals, but these mainly concentrate on the face-centered cubic (FCC) metals, especially copper and its alloys.[7–9] However, the research on the deformation behavior of HCP metals is still insufficient, and many phenomena need revealing urgently.[10,11] Magnesium (Mg), as a typical HCP structural material, has been widely used in the traffic-vehicle, aviation, and industry field in recent years as a result of its excellent properties of low density and high strength ratio. These prominent performances motivate researchers to extend the application of Mg and its alloys. Unfortunately, for Mg alloys, the plasticity at room temperature is poor due to the HCP structure coupled with low stacking fault energy. These inherent material properties restrict greatly the practical utility of Mg alloys in various fields.[12,13] The deformation behavior and strengthening mechanism of HCP structured metals are obviously different from those of the metals with FCC structure. In the past several years, a great number of investigations have proposed that low-cost Mg rare earth alloys can improve the plasticity of Mg alloys.[14,15] However, the mechanical properties of Mg alloys are still far from the expected requirements for alloying. Therefore, it is vital to search for an effective new method or technology to improve the plasticity of Mg and its alloys.

In the last few years, amorphous metallic alloys, or the so-called metallic glasses (MGs), have emerged as a new category of advanced materials. The striking properties of MGs are extraordinary yield strength, elastic strain, and wear

*Project supported by the National Natural Science Foundation of China (Grant No. 11572259), the Natural Science Foundation of Shaanxi Province, China (Grant Nos. 2018JM101 and 2019JQ-827), and the Program for Graduate Innovation Fund of Xi'an Shiyou University, China (Grant No. YCS19111004).

†Corresponding author. E-mail: gsfshy@sohu.com
‡Corresponding author. E-mail: liyulong@nwpu.edu.cn

© 2020 Chinese Physical Society and IOP Publishing Ltd

resistance.[16–18] The shear transformation zone (STZ) and shear bands (SBs) are important deformation behavior affecting the mechanical properties of MGs, which is unlike the scenario of crystalline metals. This is responsible for their poor ductility and catastrophic failure, which hinders greatly their applications. Fortunately, micropillar compression experiments on amorphous $Pd_{77}Si_{23}$ film have shown that below a pillar diameter of 400 nm, the deformation mechanism of the sample is homogeneous deformation.[19] The nano-tension tests of MGs also indicated that there exists a critical thickness which makes the MGs exhibit good plasticity.[20,21] In addition, the study also pointed out that the properties of MGs can be improved by modifying the interface structure.[22]

Recently, a large number of dual-phase alloys, consisting of crystalline and amorphous phases, have been reported to be used as the technologically-important materials due to the outstanding mechanical properties of these alloys. For example, the crystalline phase was introduced into the amorphous phase to form MGs matrix composites, which significantly improves the plasticity of amorphous alloys with large size due to multiple SBs' interactions.[23,24] On the one hand, the amorphous-crystalline interfaces (ACI) can activate the nucleation of SBs, and on the other hand, it can impede the propagation of the catastrophic SBs, thus promoting the homogeneous plastic deformation of amorphous materials, and the dual-phase composites exhibit a combination of high strength and ductility.[25] Drawing on the idea of improving MGs plasticity, the question is raised whether the dual-phase nanostructured Mg alloys (DPMAs) into which the small-sized amorphous phase with good plasticity are introduced, can ameliorate the mechanical properties of Mg alloys. For this purpose, we first proposed a crystalline/amorphous DPMA model and found that the model can improve the plasticity of Mg alloys, which is attributed to the unconventional plastic deformation mechanism.[26] Wu *et al.* have achieved great success in preparing a DPMA thin film with near-ideal strength through magnetron-sputtering technology.[27] Therefore, we also studied the effect of amorphous boundary (AB) spacing on the plastic deformation mechanism of the DPMA.[28,29] The optimal matching relationship between the size of amorphous phase and that of crystalline phase is obtained. However, the relationship between the strength and plasticity of DPMA still needs further studying. The purpose of the present work is to explore an approach to improving the tensile ductility of DPMA without sacrificing excellent strength, which serves as an advanced theory for designing and developing the high-performance dual-phase nanostructured HCP metals. For dual-phase structured metals, two factors are considered to achieve this goal: one is to improve the strength by changing the microstructure of amorphous phase; the other is to strengthen the crystalline phase. Of course, the synergistic effect between the amorphous phase and the crystalline phase is very important, which can be coordinated by adjusting the size of the amorphous phase and crystalline phase. In various experimental and theoretical methods, the method of the molecular dynamics (MD) simulation proves to be useful, particularly in investigating macroscopic and microscopic phenomena of materials,[30–32] and it is reliable in revealing the strengthening mechanism and deformation mechanism of metal materials.[33] Here, the effect of the crystalline orientation, the component of the amorphous phase and AB spacing on the deformation behavior of DPMA under tensile loading are investigated by the MD simulation method. The results show that the DPMA can obtain a superior combination of strength and plasticity by optimizing the microstructure of the dual-phase nanostructured model.

2. Simulation model and method

In this paper, the DPMA model consists of Mg crystalline phase and MgAl amorphous phase in our atomic simulation. The deformation behavior of MgAl MG has been studied in recent years.[22] Here, for simplicity, the composition of the amorphous phase in DPMAs is $Mg_{50}Al_{50}$ or $Mg_{20}Al_{80}$. The crystalline phase of each sample is composed of four grains with a columnar structure, and the amorphous phase separates the crystalline grains as a boundary. The initial configuration of the DPMA is shown in Fig. 1(a), where d represents the AB spacing. Figure 1(b) gives the DPMA sample prepared by magnetron sputtering method,[27] and it is obvious that the nanocrystalline grains embedded in the Mg-rich amorphous shell. Here, two kinds of DPMA models are proposed. Four crystalline grains of the first DPMA model have different crystalline orientations (*i.e.*, the crystalline Mg with different crystalline orientations is combined with the $Mg_{20}Al_{80}$ amorphous phase), and those of the second DPMA model have the same crystalline orientation (namely, the crystalline Mg with identical crystalline orientation is combined with $Mg_{50}Al_{50}$ amorphous phase).

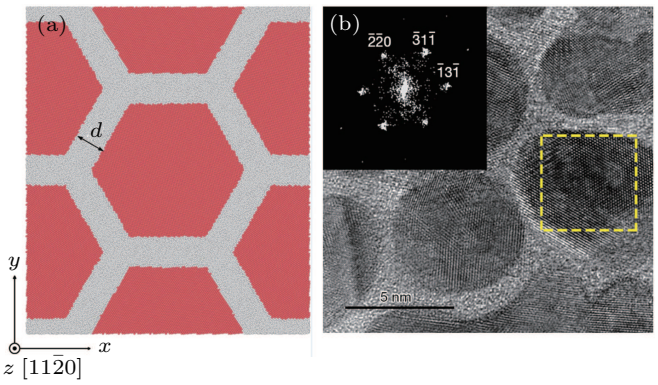


Fig. 1. (a) Atomic configuration of DPMA model. The red and gray atoms denote crystalline and amorphous phase atoms, respectively, (b) DPMA sample prepared by magnetron sputtering method,[27] with nanocrystal being marked by yellow dashed line.

For the first DPMA model, each grain rotates a certain angle around the Z axis, which is similar to previous models of nano-polycrystal Mg.[34,35] In order to investigate the effect of AB spacing on the deformation behavior of the first DPMA model, the samples with AB spacing of 1.0, 3.0, 5.0, 7.0, 8.0, and 9.0 nm are constructed, respectively. In addition, to explore whether the strengthening of the crystalline phase can improve the mechanical properties of DPMA, the effect of crystalline orientation on the second DPMA model is systematically investigated for convenience. That is to say, the strength of the crystalline phase in the second DPMA model is enhanced by changing the orientation of the crystal. Here, four crystalline grains in the second DPMA model rotate the same angle around Z axis, such as 0°, 11.25°, 33.75°, 56.25°, 78.75°, and 90°. The dimension for each of all samples is approximately 45.0 nm×52.0 nm×1.9 nm. The dimension of this model is comparable to that of the DPMA material, which is obtained through magnetron sputtering method.[27]

The selection of potential function plays an important role in MD simulation, which determines the accuracy of the calculation results. Here, the embedded atom method (EAM) potential function is used to describe the interatomic interactions of Mg–Mg, Al–Al, and Mg–Al in the simulation.[36] The periodic boundary condition (PBC) is applied to all three directions to eliminate surface effects. The atomic-scaled structures of the samples and their evolutions during the tensile deformation are analyzed by common neighbor analysis (CNA) and von Mises atomic shear strain in terms of the local structure of the atoms, utilizing the Open Visualization Tool (OVITO) software.[37] According to the local structure of the atoms, the lattice defects of the crystalline phase, such as dislocation, stacking fault and twin boundary, are discerned by CNA. The microstructures of DPMA model are identified, in which the HCP atoms, FCC atoms, and other structured atoms are colored red, green, and gray, respectively. To capture deformation behavior and describe the mechanical properties of the amorphous phase, the Von Mises atomic shear strain is used to visualize the microscopic evolution and shear strain conditions of amorphous phase atoms. The stress is calculated by the Virial theorem, which is commonly used in atomistic simulations.[38] A constant tensile strain of 5×10^{-4} is applied to the Y direction of the sample. The simulation is performed at a constant temperature of 300 K.

3. Results and discussion

3.1. Effect of amorphous phase

Previous studies have systematically investigated the mechanical behavior of the DMPA with $Mg_{50}Al_{50}$ amorphous phase.[26,29] The results show that the improvement of the plasticity of DMPA is at the expense of the strength of the alloys. Therefore, it is considered whether the sacrifice of the strength of DMPA can be reduced by changing the microstructure of amorphous phase while maintaining excellent plasticity, thus obtaining the DMPA with high strength and superior plasticity. First of all, the effect of the component of the amorphous phase on the mechanical properties of MG is investigated. Here, the alloys of $Mg_{50}Al_{50}$ MG and $Mg_{20}Al_{80}$ MG are considered. The mechanical response to the strain of the $Mg_{50}Al_{50}$ MG and the $Mg_{20}Al_{80}$ MG are shown in Fig. 2.

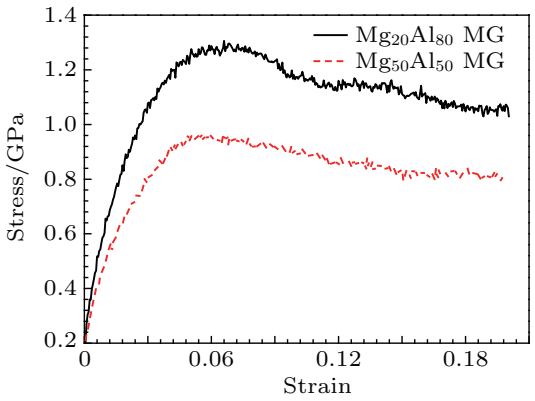


Fig. 2. Stress–strain curve of $Mg_{50}Al_{50}$ MG and $Mg_{20}Al_{80}$ MG.

It can be seen from Fig. 2 that the strength of $Mg_{20}Al_{80}$ MG is obviously higher than that of $Mg_{50}Al_{50}$ MG. On the one hand, the local structure around the Mg trends to be maintained as fragments when Al content is less. With the increase of Al atoms, the fragments of Mg are eventually disaggregated into the discrete Mg atoms. Therefore, the atomic structure of Mg and Al in $Mg_{50}Al_{50}$ tend to concentrate in some local regions and the uniform distribution of Mg atoms and Al atoms are revealed in $Mg_{20}Al_{80}$.[39] According to Zhou *et al.*,[40] the region where the Al and Mg atoms are concentrated is considered to be a weak zone, and defects may be preferentially generated. On the other hand, this may be attributed to the fact that the MgAl MG is mainly composed of icosahedral-related clusters with Al as the central atom, which is disorderly connected. Like CuZr MG, the $Mg_{20}Al_{80}$ has more Al-centered icosahedra and exhibits a greater strength, *i.e.*, higher resistance to the initiation of flows but an increased propensity to strain localization, which $Mg_{50}Al_{50}$ is opposite to. As a consequence, the first DPMA model with the amorphous phase of $Mg_{20}Al_{80}$ is established to explore the mechanical behavior of the DPMA with excellent strength and plasticity. In order to obtain the optimal matching relationship between AB spacing and the crystalline phase size of DPMA, the effect of AB spacing on the deformation behavior of the first DPMA model is investigated. Here, the AB spacing is 1.0, 3.0, 5.0, 7.0, 8.0, and 9.0 nm, respectively. The stress–strain curves corresponding to the samples with various AB spacing are given in Fig. 3(a). Additionally, it has been confirmed that for the first DPMA model, when the AB spacing

reaches 5.0 nm, the sample exhibits superior plasticity.[26,29] For comparison, the stress–strain curve of the first DPMA model with the amorphous phase of $Mg_{50}Al_{50}$ is also given in Fig. 3(a).[29] When the AB spacing is 5.0 nm, the peak stress of the $Mg_{50}Al_{50}$ DPMA model is 1.34 GPa and that of the $Mg_{20}Al_{80}$ DPMA model can achieve 1.57 GPa. That is to say, when the amorphous phase of $Mg_{20}Al_{80}$ is used instead of the amorphous phase of $Mg_{50}Al_{50}$ in the DPMA, the strength of alloys increases by 17.2%. In addition, it can be observed in Fig. 3(a) that when the AB spacing is larger than 5.0 nm, the deformation-induced stress drops, almost disappear for the $Mg_{20}Al_{80}$ DPMA model and the nearly perfect plastic flow behavior occurs during plastic deformation. In other words, the samples with large AB spacing exhibit perfect plasticity. Consequently, the results confirm that the strength of DPMA can be greatly enhanced while the superior plasticity is maintained by changing the microstructure of the amorphous phase. And the curves in Fig. 3(a) show that all the DPMA models first deform elastically until shortly before the stress reaching the peak stress, and the flow behaviors deviate from the linear relationship after onset of plastic deformation. It is apparent that the peak stress of the $Mg_{20}Al_{80}$ DPMA model is closely related to AB spacing. In detail, the peak stresses of the $Mg_{20}Al_{80}$ DPMA samples with the AB spacing of 1.0, 3.0, 5.0, 7.0, 8.0, and 9.0 nm are 1.81, 1.71, 1.57, 1.53, 1.50, and 1.47 GPa, respectively. Namely, the peak stress of the sample decreases with the increase of AB spacing. It may be attributed to the fact that the crystalline phase acts as the hard phase in the DPMA. The proportion of the crystalline phase is higher for the samples with smaller AB spacing, behaving as the reinforcement phase, therefore the ability to resist the shear deformation is improved. Of course, the synergistic interaction between the crystalline phase and the amorphous phase also plays an important role in enhancing the strength of DPMA.

During the whole deformation stage, τ_y reflects the peak stress while τ_S can be regarded as the average flow stress of the sample. Here, the average flow stress at the strain between 0.15 and 0.20 is calculated for all samples. The difference between τ_y and τ_S lies in the stress drop ($\Delta\tau = \tau_y - \tau_S$). As shown in Fig. 3(a), when the AB spacing is 1.0 nm and 3.0 nm, the $Mg_{20}Al_{80}$ DPMA model exhibits the abrupt stress drop. However, with the further increase of AB spacing, the deformation-induced stress drops almost vanish. In our simulation, we define $\rho = \tau_y/\Delta\tau$ as a parameter to evaluate the plasticity of the DPMA. The larger value of ρ indicates that the sample has better plasticity.[41,42] For the $Mg_{20}Al_{80}$ DPMA model, the values of ρ with AB spacing of 1.0, 3.0, 5.0, 7.0, 8.0, and 9.0 nm are 2.33, 4.54, 6.67, 8.33, 9.09, and 11.11, respectively. According to the values of τ_y and ρ of the samples, the mechanical properties of the DPMA are representatively characterized in Fig. 3(b). Previous study has shown that for the $Mg_{50}Al_{50}$ DPMA model, when the AB spacing is 5.0 nm, the plasticity of the sample is excellent.[29] Here, for comparison, the values of τ_y and ρ of the $Mg_{50}Al_{50}$ DPMA models in the previous study are also given in Fig. 3(b). The AB spacing values of these samples are 3.0, 5.0, and 7.0 nm, respectively. As can be clearly described from Fig. 3(b), each of the $Mg_{20}Al_{80}$ DPMA models in regime I has excellent strength but poor plasticity. While for the samples within the regime II, although the strength of the $Mg_{20}Al_{80}$ DPMA model decreases slightly, the samples each possess great strength and superior plasticity compared with the $Mg_{50}Al_{50}$ DPMA model, as indicated by the grey ellipse. This probably means that the $Mg_{20}Al_{80}$ DPMA models in regime I and regime II possess different plastic deformation mechanisms. Present in regime III is only the $Mg_{50}Al_{50}$ DPMA model with the AB spacing of 7.0 nm, which exhibits extremely low strength. In addition, it can be concluded from Fig. 3(b) that the peak stress of the $Mg_{20}Al_{80}$ DPMA model is better than that of the $Mg_{50}Al_{50}$ DPMA model at the same AB spacing. The results indicate that the $Mg_{20}Al_{80}$ DPMA model has a more attractive integration of outstanding mechanical properties. In other words, the strength of the DPMA can be improved by strengthening the amorphous phase, and the DPMA with excellent strength and superior plasticity can be obtained.

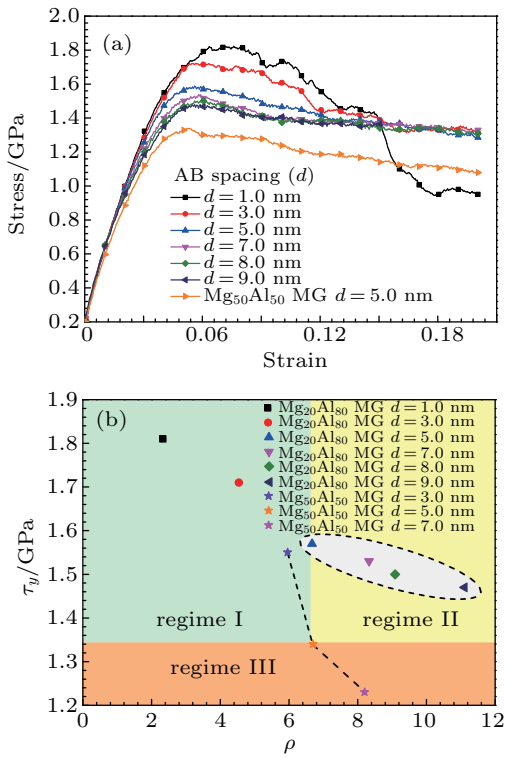


Fig. 3. (a) Typical stress–strain curves of the first DPMA model with varying AB spacing, and (b) comparison among curves of τ_y *versus* ρ of the first DPMA model.

For the potential plastic deformation behavior of the $Mg_{20}Al_{80}$ DPMA model, the atomic snapshots of the samples with various AB spacing under different strains are shown in Figs. 4 and 5. The atomic configurations of the $Mg_{20}Al_{80}$

DPMA model with the AB spacing of 1.0 nm are exhibited in Fig. 4. At the preliminary stage of plastic deformation, the basal dislocation nucleated from ACI is emitted into the grain interior as shown in Fig. 4(a). As the applied strain increases, the significant stress drop in the stress–strain curve corresponds to the generation and growth of basal/prismatic (BP) interface (*i.e.*, the generation and growth of the new grains mentioned in our previous literature[26,43,44]), which is caused by atomic rearrangement as shown in Fig. 4(b). Ultimately, as the strain increases up to 0.20, the new grains almost completely engulf the entire matrix grains. Simultaneously, the stacking faults occur due to the partial dislocations emitted along the slip plane within grains. The result shows that as the strain increases, the capacity of the amorphous phase in the $Mg_{20}Al_{80}$ DPMA model to accommodate plastic deformation is insufficient when the AB spacing is small, the deformation mechanism of the sample is dominated by dislocations slipping and new grains forming in the later stage of plastic deformation.

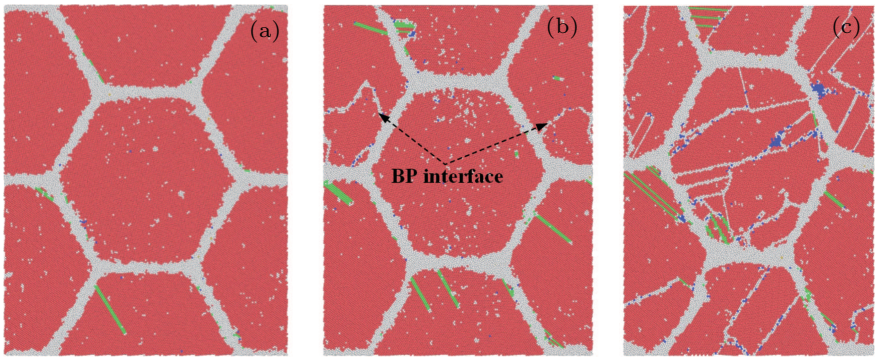


Fig. 4. Snapshots of $Mg_{20}Al_{80}$ DPMA model with AB spacing of 1.0 nm under the strain of (a) 0.05, (b) 0.11, and (c) 0.20.

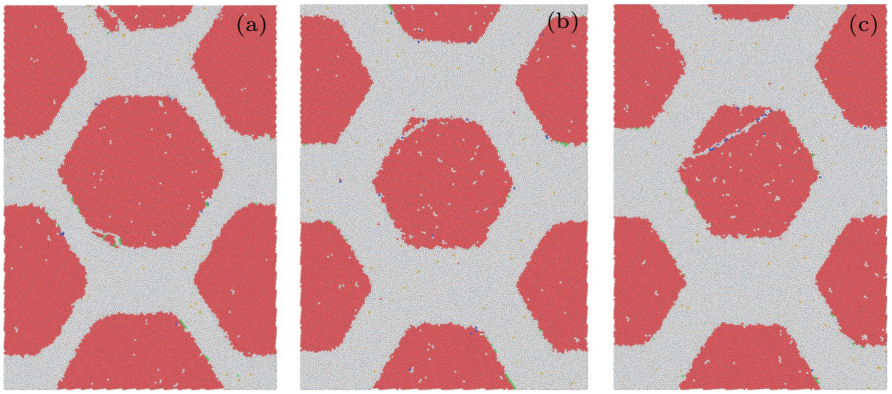


Fig. 5. (a) Atomic configuration of $Mg_{20}Al_{80}$ DPMA model with AB spacing of 5.0 nm under the strain of 0.20. Atomic configurations of the $Mg_{20}Al_{80}$ DPMA model with the AB spacing of 8.0 nm under the strain of (b) 0.14 and (c) 0.20, respectively.

Figure 5 shows the atomic configurations of the $Mg_{20}Al_{80}$ DPMA model with larger AB spacing. Figure 5(a) clearly shows that there are a few stacking faults in the crystalline phase, caused by the dislocation slipping near the ACI, which is attributed to the local stress imbalance at the ACI interface. Moreover, the stacking faults appear in the early stage of the $Mg_{20}Al_{80}$ DPMA model deformation, and the slip of other dislocations is not found with the further increase of strain. Namely, the contribution of the crystalline phase to the plastic deformation of the sample can be neglected. This indicates that the plastic deformation mechanism of the $Mg_{20}Al_{80}$ DPMA model with the AB spacing of 5.0 nm is almost completely dependent on the deformation of the amorphous phase. This is in reasonably good consistence with previous studies.[26,29,45] What is interesting is that when the AB spacing increases to 8.0 nm, the new grain is formed in the crystalline phase of the $Mg_{20}Al_{80}$ DPMA model under the strain of 0.14 as shown in Fig. 5(b). However, compared with the growth of grain in the $Mg_{20}Al_{80}$ DPMA model with the AB spacing of 1.0 nm, the growth of new grain is very slow as shown in Fig. 5(c). Does this imply the conversion of the deformation mechanism of the $Mg_{20}Al_{80}$ DPMA model?

To further reveal the transformation of the deformation mechanism of the $Mg_{20}Al_{80}$ DPMA model with the increase of AB spacing, the atomic shear strain snapshots of the samples with the AB spacing of 3.0 nm and 8.0 nm under different strains are presented, and atoms colors refer to the shear strain for clarity as shown in Fig. 6. The red atom means higher atomic shear strain, and the blue atom refers to lower atomic shear strain. For the $Mg_{20}Al_{80}$ DPMA model with the AB

spacing of 3.0 nm, at the initial stages of plastic deformation, some STZs are activated near the ACI due to stress concentration. With the increase of strain, STZs occupy the whole amorphous phase. The ability of small-sized amorphous phase to undertake plastic deformation is limited, so the emission of dislocations and the nucleation of new grains occur in the crystalline phase as shown in Fig. 6(a). However, as shown in Fig. 6(b), for the $Mg_{20}Al_{80}$ DPMA model with the AB spacing of 8.0 nm, as the strain increases, the new grains appear again in the crystalline phase. This may be attributed to the fact that with the increase of AB spacing, the amorphous phase has larger space, which makes it easier for STZs to aggregate and form mature SBs. The SBs interact with and "pinned" to each other, causing pronounced stress to concentrate, ultimately resulting in the formation of new grains near the intersection of SBs, which is observed in Figs. 5(b) and 6(b). For the $Mg_{20}Al_{80}$ DPMA model with the AB spacing of 5.0 nm, a transition mechanism takes effect. Since the AB spacing is not large enough to cause the STZs to aggregate into SBs and the amorphous phase is just enough to undertake the plastic deformation of the sample, the crystalline phase of the $Mg_{20}Al_{80}$ DPMA model does not participate in the plastic deformation and no new grains appear in the crystalline phase. Therefore, the $Mg_{20}Al_{80}$ DPMA model with the AB spacing of 5.0 nm exhibits a superplastic deformation behavior, which can possess brilliant plasticity without sacrificing strength.

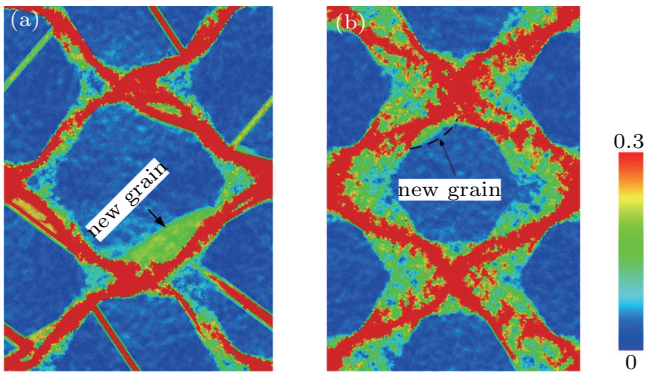


Fig. 6. (a) Snapshot of the $Mg_{20}Al_{80}$ DPMA model (a) with AB spacing of 3.0 nm under strain of 0.12, and (b) with AB spacing of 8.0 nm under strain of 0.14.

3.2. Effect of crystalline phase

As mentioned above, changing the microstructure (*i.e.*, strength) of the amorphous phase can enhance the strength of DPMA while its plasticity is maintained. Can the mechanical properties of DPMA be improved by enhancing the strength of the crystalline phase? In order to pursue an alternative approach to improving the strength of Mg alloys while excellent plasticity is maintained, an ideal model of DPMA with the same crystalline orientation (*i.e.*, the second DPMA model) is established. Here, to compare with the previous work, the amorphous phase of the second DPMA model, *i.e.*, $Mg_{50}Al_{50}$, is adopted. It is worth noting that the strength of the crystalline phase is here adjusted by changing the orientation of the crystalline grains. This is achieved by rotating the crystalline phase at a certain angle, that is, four crystalline grains in the $Mg_{50}Al_{50}$ DPMA model have the same crystalline orientation, and rotate the same angle around the Z axis. The rotation angle is θ, and θ is 0°, 11.25°, 33.75°, 56.25°, 78.75°, and 90°, respectively. Firstly, when the AB spacing is 5.0 nm, the effect of rotation angle (*i.e.*, crystalline orientation) on the mechanical properties of the $Mg_{50}Al_{50}$ DPMA model is investigated. Figure 7(a) shows the stress–strain curves of the $Mg_{50}Al_{50}$ DPMA model with different rotation angles under tensile loading. The results indicate that the peak stress of the $Mg_{50}Al_{50}$ DPMA model greatly depends on crystalline orientation. This illustrates that the mechanical properties of DPMA can be improved by enhancing the strength of the crystalline phase. It is formulated in Fig. 7(a) that when the rotation angle is 90°, the $Mg_{50}Al_{50}$ DPMA model has the strongest peak stress and the value is 1.39 GPa. This is due to the fact that the loading direction is perpendicular to the basal plane of the crystalline phase when the rotation angle is 90° and the Schmidt factor tends to be 0.0. Moreover, according to the above analysis, all the samples have the advantages of excellent plasticity as shown in Fig. 7(a). In order to investigate the effect of AB spacing on the deformation behavior of the maximum strength model, the stress–strain curves of the 90° samples with the AB spacing of 1.0, 2.0, 3.0, 4.0, and 5.0 nm are shown in Fig. 7(b). For comparison, the curves of the first $Mg_{50}Al_{50}$ DPMA model in previous literature are also given, in which the orientations of four grains are different.[29] The AB spacing of the first $Mg_{50}Al_{50}$ DPMA model is 5.0 nm and 7.0 nm, separately. It reveals that the second $Mg_{50}Al_{50}$ DPMA model exhibits the abrupt stress drop when the AB spacing is small. For the samples with the AB spacing of 4.0 nm and 5.0 nm, the sudden drop in stress disappears. Here, the mechanical properties of the 90° DPMA models are characterized by calculating the value of ρ of each sample. When AB spacing is 4.0 nm, the ρ of the 90° DPMA model is 8.10. It reveals that the sample with the AB spacing of 4.0 nm has brilliant plasticity. For comparison, the ρ value of the first $Mg_{50}Al_{50}$ DPMA model with the AB spacing of 5.0 nm and 7.0 nm are also calculated, which is 6.7 and 8.2 separately. Additionally, as shown in Fig. 7(b), the peak stress of the 90° DPMA model is 1.39 GPa when the AB spacing is 5.0 nm. At the same AB spacing, it is 3.7% greater than the peak stress of the first $Mg_{50}Al_{50}$ DPMA model. Meantime, based on the stress–strain curves, when AB spacing reaches the critical value, such as 4.0 nm, the 90° DPMA model exhibits superplastic deformation behavior. It is very striking that compared with the previous results, the

AB spacing decreases when the 90° $Mg_{50}Al_{50}$ DPMA model exhibits superplastic deformation behavior by enhancing the strength of the crystalline phase.[29] This might be due to the fact that strengthening crystalline phase can greatly promote the resistance of crystalline phase to plastic deformation. When the AB spacing reaches the critical value, the plastic deformation mechanism of the DPMA mainly depends on the deformation of the amorphous phase, and the DPMA exhibits perfect plasticity. However, the critical value is related to the strength and plasticity of the amorphous phase and crystalline phase. Therefore, by adjusting the strength of the amorphous phase and crystalline phase and optimizing the AB spacing, the DPMA with both excellent strength and perfect plasticity can be produced. This result is conductive to improving the strength of the DPMA by strengthening the crystalline phase while its plasticity is maintained. Additionally, according to Wu *et al.*'s research,[27] $MgCu_2$ can be used as the reinforcing phase to obtain the ultra-high-strength DPMA. Therefore, it is assumed that the DPMA with excellent strength and plasticity can be obtained by taking $MgCu_2$ with high strength as the crystalline phase and adjusting the size of amorphous and crystalline phase appropriately.

For the better revealing of the deformation mechanism of DPMA, figure 8 exhibits the deformation snapshots of the 90° $Mg_{50}Al_{50}$ DPMA model with different AB spacing under various strains. As shown in Figs. 8(a)–8(c), the pyramidal $\langle c+a \rangle$ dislocations are observed in the preliminary stage of plastic deformation for the sample with small AB spacing. When the strain increases to 0.07, the appearance of the BP interface (*i.e.*, the nucleation of new grain) is observed, which corresponds to the significant stress drop on the stress–strain curve. Moreover, Luo *et al.* suggested that the accumulation of local stress at the triple junction of polycrystalline metal is called back stress, which can activate the nucleation of defects.[46] In our simulation, the observations can be explained by the fact that when the AB spacing is small enough, the back stress at the triple junction may reach the critical value and new grains are preferentially activated in the grain opposite the triple junction as shown in Fig. 8(a). As the strain goes up to 0.20, the new grains almost completely penetrate the entire matrix grains. This may be because when the tensile loading is perpendicular to the basal plane of crystalline Mg, the slip of basal plane is restricted, thus pyramidal slips, new grains, and BP interfaces occur in the crystalline phase. For the sample with the AB spacing of 4.0 nm, it is evident in Fig. 8(d) that even if the strain reaches to 0.20, there are only a few basal stacking faults that can be observed in the crystalline phase. Previous studies have suggested that the nucleation and propagation of SBs occur in amorphous phase with the increase of strain when AB spacing increases to a critical value in the second $Mg_{50}Al_{50}$ DPMA model. The critical resolved shear stress of the basal dislocation is very small, the movement of atoms in SBs in amorphous phase results in the nucleating and slipping of the basal dislocations, which leads the basal stacking faults to occur in the crystalline phase.

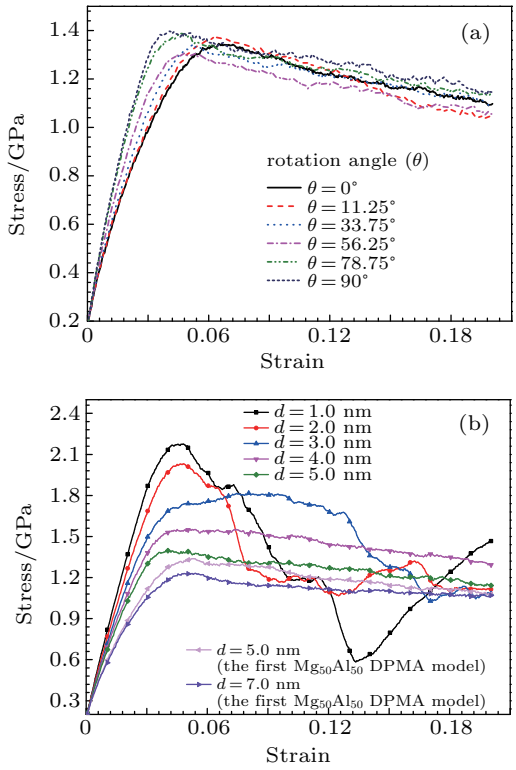


Fig. 7. Stress–strain curves of the second DPMA model (a) with various rotation angles when AB spacing is 5.0 nm, and (b) with various AB spacings when rotation angle is 90°.

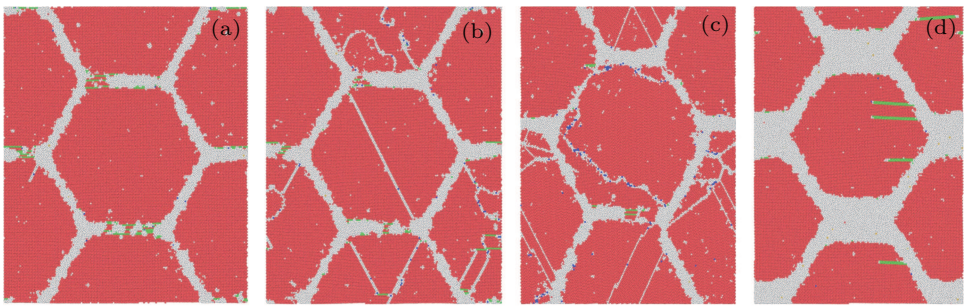


Fig. 8. Atomic configurations of 90° $Mg_{50}Al_{50}$ DPMA model with AB spacing of 2.0 nm under the strain of (a) 0.04, (b) 0.07, and (c) 0.20. (d) Atomic configuration of the 90° $Mg_{50}Al_{50}$ DPMA model with AB spacing of 4.0 nm under strain of 0.20.

In addition, when AB spacing is 5.0 nm, the mechanical property of the 90° $Mg_{20}Al_{80}$ DPMA model is also investigated. Figure 9 shows the stress–strain curve of the 90° $Mg_{20}Al_{80}$ DPMA model and the 90° $Mg_{50}Al_{50}$ DPMA model. It is clearly demonstrated from Fig. 9 that the 90° $Mg_{20}Al_{80}$ DPMA model exhibits greater strength while its excellent plasticity is maintained. Research results further confirm that by adjusting the strength of the amorphous phase, the strength of the DPMA can be significantly improved while its excellent plasticity is maintained when the strength of the crystalline phase is constant. Of course, the superplastic deformation of DPMA can be obtained by increasing the AB spacing. Namely, for the DPMA model, when the amorphous phase (or crystalline phase) is strengthened, it is necessary to increase (or reduce) the AB spacing to achieve superior plasticity. The above research clearly reveals that the mechanical properties of the DPMA can be significantly improved by strengthening both crystalline phase and amorphous phase as well.

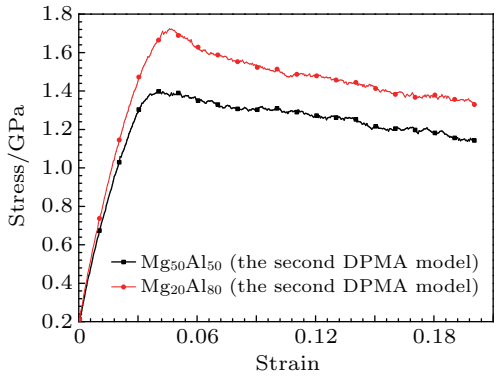


Fig. 9. Stress–strain curve of 90° $Mg_{50}Al_{50}$ and 90° $Mg_{20}Al_{80}$ DPMA model when AB spacing is 5.0 nm.

4. Conclusions

The effect of the crystalline orientation, the component of the amorphous phase and AB spacing on the mechanical properties of DPMA under tensile loading are investigated by the MD simulation method. The results indicate that compared with the previous results, the strength of the first DPMA model increases by 17% while its excellent plasticity is maintained. In other words, the strength of the DPMA can be improved by strengthening the amorphous phase. For the first DPMA model, with the increase of AB spacing, the plastic deformation mode changes from the generation of dislocations and new grains in the crystalline phase to the plastic deformation dominated almost entirely by amorphous phase. What is interesting is that when the AB spacing further increases to 8.0 nm, the new grain is again formed in the crystalline phase of the first DPMA model due to the interaction with and "pinned" of SBs to each other in the amorphous phase. However, comparing with the sample with small AB spacing, the growth of new grain is very slow, and the plastic deformation of the sample is still mainly the amorphous phase. The results also show that by adjusting the strength of the crystalline phase, the strength of the DPMA can also be obviously improved while the good plasticity is maintained. This might be due to the fact that strengthening the crystalline phase can greatly promote the resistance to the plastic deformation of crystalline phase. The results further indicate that for the DPMA model, when the amorphous phase (or crystalline phase) is strengthened to enhance its strength, the AB spacing must be increased (or reduced) to obtain its excellent plasticity at the same time. Namely, the strength of DPMA can be significantly improved while its excellent plasticity is maintained by adjusting the strength of the amorphous phase or crystalline phase and optimizing the AB spacing. The present work provides a strong theoretical basis and reference for designing and developing the high-performance dual-phase HCP nanostructured metals material.

References

[1] Wang Y, Chen M, Zhou F and M E 2002 *Nature* **419** 912
[2] Liao M, Li B and Horstemeyer M F 2013 *Comput. Mater. Sci.* **79** 534
[3] Gliiter H, Schimmel T and Hahn H 2014 *Nano Today* **9** 17
[4] Hao L H, Liu Q, Fang Y Y, Huang M, Li W, Lu Y, Luo J F, Guan P F, Zhang Z, Wang L H and Han X D 2019 *Comput. Mater. Sci.* **169** 109087
[5] Li X and Lu K 2019 *Science* **364** 733
[6] Rajulapati K, Scattergood R, Murty K, Duscher G and Koch C 2006 *Scr. Mater.* **55** 155
[7] Song H Y, Wang M, Deng Q and Li Y L 2018 *J. Non-Cryst. Solids* **490** 13
[8] Lu B K and Wang C Y 2018 *Chin. Phys. B* **27** 077104
[9] An M R, Song H Y and Su J F 2012 *Chin. Phys. B* **21** 106202
[10] Song H Y and Li Y L 2016 *Chin. Phys. B* **25** 026802
[11] Chang L, Zhou C Y, Li J and He X H 2018 *Comput. Mater. Sci.* **142** 135
[12] Li G M, Wang Y B, Xiang M Z, Liao Y, Wang K and Chen J 2018 *Int. J. Mech. Sci.* **141** 143
[13] Alaneme K K and Okotete E A 2017 *J. Magnes. Alloy* **5** 460
[14] Silva C J, Kula A, Mishra R K and Niewczas M 2018 *J. Alloys Compd.* **761** 58
[15] Tang L, Liu W, Ding Z, Zhang D, Zhao Y, Lavernia E J and Zhu Y 2016 *Comput. Mater. Sci.* **115** 85
[16] Qiao J C, Wang Q, Crespo D, Yang Y and Pelletier J M 2017 *Chin. Phys. B* **26** 016402
[17] Tang C and Wong C H 2015 *Intermetallics* **58** 50
[18] Jiang S Q, Huang Y and Li M Z 2019 *Chin. Phys. B* **28** 046103
[19] Volkert C A, Donohue A and Spaepen F 2008 *J. Appl. Phys.* **103** 083539
[20] Zhao P, Li J and Wang Y 2014 *Acta Mater.* **73** 149
[21] Albe K, Pitter Y and Sopu D 2013 *Mech. Mater.* **67** 94
[22] Zhou X and Chen C 2016 *Int. J. Plast* **80** 75
[23] Guo W, Jägle E, Yao J, Maier V, Korte-Kerzel S, Schneider J M and Raabe D 2014 *Acta Mater.* **80** 94
[24] Zhao L, Chan K C and Shen S H 2018 *Intermetallics* **95** 102
[25] Liu M C, Lee C J, Lai Y H and Huang J C 2010 *Thin Solid Films* **518** 7295
[26] Song H Y and Li Y L 2015 *Phys. Lett. A* **379** 2087
[27] Wu G, Chan K C, Zhu L, Sun L and Lu J 2017 *Nature* **545** 80
[28] Song H Y, Dai J L, An M R, Xiao M X and Li Y L 2019 *Comput. Mater. Sci.* **165** 88

[29] Song H Y, Zuo X D, An M R, Xiao M X and Li Y L 2019 *Comput. Mater. Sci.* **160** 295
[30] Wang T W, Li X, Wu Q Q, Jiao T F, Liu X Y, Sun M, Hu F L and Huang D C 2018 *Chin. Phys. B* **27** 124704
[31] Cui S W, Wei J A, Liu W W, Zhu R Z and Qian P 2019 *Chin. Phys. B* **28** 016801
[32] Wang C Y, Lu S, Yu X D and Li H P 2019 *Chin. Phys. B* **28** 016501
[33] Wolf D, Yamakov V, Phillpot S R, Mukherjee A and Gleiter H 2005 *Acta Mater.* **53** 1
[34] Kim D H, Manuel M V, Ebrahimi F, Tulenko J S and Phillpot S R 2010 *Acta Mater.* **58** 6217
[35] Song H Y, Zuo X D, Yin P, An M R and Li Y L 2018 *J. Non-Cryst. Solids* **494** 1
[36] Liu X Y, Ohotnicky P P, Adams J B, Rohrer C L and Jr R W H 1997 *Surf. Sci.* **373** 357
[37] Stukowski A 2010 *Modell. Simul. Mater. Sci. Eng.* **18** 015012
[38] Cheung K S and Yip S 1991 *J. Appl. Phys.* **70** 5688
[39] Wang J, Li X, Pan S and Qin J 2017 *Comput. Mater. Sci.* **129** 115
[40] Zhou X and Chen C 2016 *Comput. Mater. Sci.* **117** 188
[41] Peng C X, Şopu D, Cheng Y, Song K K, Wang S H, Eckert J and Wang L 2019 *Mater.* **168** 107662
[42] Kim H K, Lee M, Lee K R and Lee J C 2013 *Acta Mater.* **61** 6597
[43] Song H Y, Zhang K, An M R, Wang L, Xiao M X and Li Y L 2019 *J. Non-Cryst. Solids* **521** 119550
[44] Song H Y and Li Y L 2012 *J. Appl. Phys.* **112** 054322
[45] Song H Y, Wang J Y, An M R, Xiao M X and Li Y L 2019 *Comput. Mater. Sci.* **162** 199
[46] Luo H B, Sheng H W, Zhang H L, Wang F Q, Fan J K, Du J, Liu J P and Szlufarska I 2019 *Nat. Commun.* **10** 3587